

Pulse Compression for Ultrafast Nonlinear Microscopy

White Paper

Revision 1.2
June 2015

When shorter laser pulses are better...

It has been established that optical techniques based on nonlinear processes, such as two-photon excited fluorescence (TPEF) and second harmonic generation (SHG), are advantageous for microscopic imaging at depth [1-4]. When compared with confocal or wide-field microscopy techniques, they provide greater penetration depths and superior image contrast. The nonlinear optical response to a focused laser field is intrinsically confined to the focal volume, which helps mitigating light scattering effects and allows imaging at depths as large as four-five mean free path lengths [5-7]. Longer wavelength of the excitation light (usually, in near-IR domain) is also beneficial for dealing with scattering in tissues.

Multiphoton processes, in turn, favor ultrashort laser pulses because of the high peak intensity they can deliver even for relatively low energy per pulse. For instance, a 0.1-nJ (1 nJ = 10^{-9} J) pulse with full-width-at-half-maximum (FWHM) time duration of 100 fs (1 fs = 10^{-15} s) has $\sim 10^{12}$ W/cm² peak intensity when focused into 0.3- μ m spot by a high numerical aperture (NA) objective. Up to a certain limit, the nonlinear excitation efficiency is simply inversely proportional to the pulse duration in $n-1$ power, where n is the order of the nonlinearity used. That is a 10-fs pulse produces an order of magnitude more TPEF photons than a 100-fs pulse of the same energy and under similar focusing conditions; see Fig. 1. Better yet, one can control the spectral phase of the pulse to selectively excite different fluorophores [8-10]; and that is without tuning the laser emission wavelength.

The anticipated question is why microscope manufacturers, such as Nikon, Olympus, and Zeiss, have largely ignored the opportunity to exploit commercially available ultra-broadband laser sources and instead opted for tunable laser

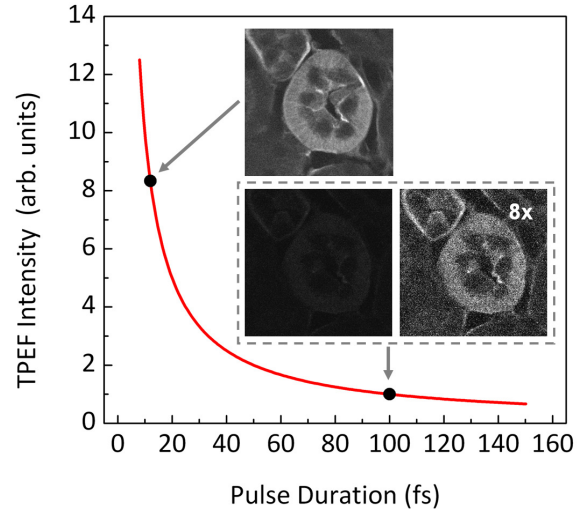


Figure 1. Expected dependence of TPEF intensity on laser pulse duration assuming the system response is instantaneous (i.e., two-photon absorption efficiency is the same throughout the pulse spectrum) and laser pulses are TL. Inset: TPEF imaging of a commercial mouse kidney slide (Molecular Probes, F-24630) with 12 fs and 100 fs laser pulses. The average laser power on the sample and other acquisition parameters are the same. The excitation spectra are centered at 810 nm. The objective used is Zeiss LD C-Apochromat 40x/1.1 NA. The net gain in signal is about 8 fold. The figure is adapted from ref. [11].

systems such as MaiTai DeepSee (SpectraPhysics, Newport) and Chameleon Vision (Coherent), with transform-limited (TL) pulse duration close to 100 fs.

Using shorter pulses is a challenge

Ultrashort pulses become increasingly sensitive to material dispersion, which can be described by nonlinear terms in the Taylor series expansion of the spectral phase $\varphi(\omega)$ about carrier frequency ω_0

$$\varphi(\omega) = \sum_{n=0}^{\infty} \frac{\varphi_n}{n!} \cdot (\omega - \omega_0)^n, \quad \varphi_n \equiv \left. \frac{d^n \varphi}{d\omega^n} \right|_{\omega=\omega_0} .$$

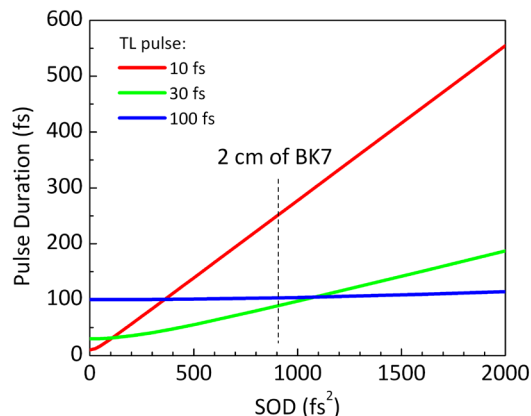


Figure 2. Dependence of the FWHM pulse duration on the amount of added SOD. The simulations assume a Gaussian spectrum, centered at 800 nm, and TL pulse duration to start with.

The effect of second-order dispersion (SOD), corresponding to coefficient ϕ_2 in the series, on the FWHM duration of an initially TL pulse is illustrated in Fig. 2. For instance, 1,000 fs² of linear chirp, acquired by a pulse after passing through ~2 cm of BK7 glass, stretches a 10-fs pulse to 277.4 fs, and a 30-fs pulse to 97.2 fs. Under the same conditions, a 100-fs pulse duration changes to 103.8 fs, *i.e.*, remains largely unaffected. The SOD of a microscope setup, primarily due to the objective, can easily exceed 4,000 fs²; see Table 1 below.

What about higher orders of dispersion? Experimentally, TL pulse durations down to 60 fs (spectral bandwidth of 15 nm, centered at 800 nm) have been restored after the objective lens by a simple prism-pair compressor [12], *i.e.*, by correcting only for SOD. The linear dependence of TPEF intensity on the bandwidth of the pump pulse has been confirmed using SOD only compensation up to 30-35 nm [13, 14]. Spectral bandwidth of 45 nm FWHM, however, requires third-order dispersion (TOD) compensation [15].

To correct for TOD, Muller et al. combined the prism-pair compressor with a properly chosen dielectric mirror assembly [16]. Fork et al. utilized a combination of prisms and

diffraction gratings [17], while Larson and Yeh reported the design of a single multi-layer mirror [18]. Grism (a grating in optical contact with a prism) is another modality that can be used to compensate for SOD and TOD simultaneously [19].

All of the approaches above have one significant practical drawback - they are static, *i.e.*, they imply meticulous tailoring of their parameters to a specific optical setup (laser and microscope objective) and the devices have to be tuned or completely redesigned if the dispersion of the system has changed due to laser alignment drifts or simply because of switching to another objective. As a result, a laser expert is needed to keep track of and counter phase changes. Maintenance time surpasses practical limits for biomedical applications. Note also that the discussed implementations are limited to correcting only SOD and TOD. Phase distortion correction beyond TOD is needed for pulses with >100 nm spectral bandwidth, or when dielectric mirrors that may have a limited window over which they maintain a relatively flat phase are used.

Table 1. Reported SOD values for whole microscope systems (sys) and single objectives (obj)

Objective	Reported SOD	Refs.
PlanNeoFluar 0.3NA, 10x	500±100 fs ² @780 nm (obj)	[20]
PlanNeoFluar 0.9NA, 40x	950±100 fs ² @780 nm (obj)	[20]
Apochromat 1.2NA, 40x	1800±100 fs ² @780nm (obj)	[20]
Apochromat 1.4NA, 63x, oil	3200±100 fs ² @780 nm (obj)	[20]
PlanNeoFluar 1.3NA, 40x, oil	1104 fs ² @800 nm (obj)	[15]
	4500±600 fs ² @800 nm (sys)	[15]
C-Apochromat 1.2NA, 63x, W	1140 fs ² @800nm (obj)	[15]
	4646±600 fs ² @800nm (sys)	[21]
	4528 fs ² @800nm (sys)	[18]
Achroplan 0.95NA, 63x	3728 fs ² @800nm (sys)	[18]

Is there a PRACTICAL solution?

Fortunately, there is. Adaptive pulse characterization and compression is possible using an optical pulse shaper. A pulse shaper is an instrument capable of manipulating phase, amplitude and in some cases, polarization of laser pulses. Many shaper designs have been explored over the years and two major concepts prevailed. One is known as a 4f shaper design [22, 23], where the light spectrum is dispersed spatially, and phase (and amplitude) changes are introduced at the Fourier plane using a spatial light modulator (SLM). Its unfolded layout is depicted in Fig. 3(a). The other is based on an acousto-optic programmable dispersive filter (AOPDF), where a traveling acoustic wave couples ordinary and extra-ordinary optical waves in a birefringent crystal and thereby imprints its pre-programmed amplitude and phase structure on the optical waveform [24-26]. The conceptual geometry of AOPDF is illustrated in Fig. 3(b).

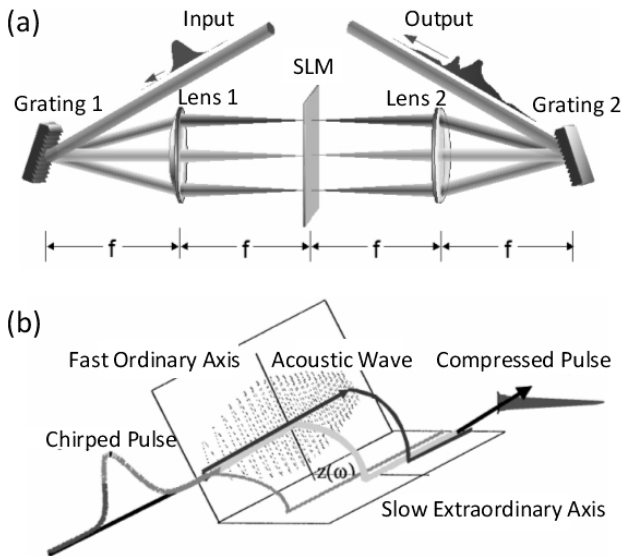


Figure 3. Two widely accepted pulse shaping concepts: (a) 4f shaper design, (b) AOPDF-based.

The 4f design has been favored by researchers for its versatility and independence on the laser repetition rate allowing shaping the

output of high-repetition-rate laser systems used for microscopy. The AOPDF-based devices are more compact due to their in-line geometry but they do require synchronization with a pulsed laser source. Because of the time it takes for an acoustic wave to travel through a few-centimeter-long crystal, the laser repetition rate has been limited to <30 kHz.

Shaper-based pulse characterization and compression methods also vary. Historically, the first introduced method was the one that bypassed the phase measurement altogether. It relied on a computer learning algorithm to optimize SHG by adding random phase distortions across the bandwidth of the pulse being compressed and monitoring the integrated SHG signal [27, 28]. The premise is that SHG intensity achieves its maximum when phase distortions are minimized; therefore, SHG optimization is equivalent to pulse compression.

A different direction in shaper-based pulse compression involves mimicking known pulse characterization techniques. For time-domain measurements, a calibrated pulse shaper is used to synthesize the required laser pulses and adjust the time delay between them to simulate common pulse measurement methods such as SHG-FROG [29, 30] and SPIDER [31]. For frequency-domain measurements, shaper-based variants of sonogram methods such as STRUT can be implemented [29, 32]. The later appear to handle better highly modulated phase distortions such as those introduced by multi-stack dielectric coatings. This has been recently demonstrated by a variant that takes full advantage of the pulse shaper and measured the sonogram in the single-beam configuration (no external reference arm) by isolating narrowband reference pulses within the input spectrum [32].

Given that pulse broadening is typically caused by group velocity dispersion, it is the non-zero second derivative of the phase that

needs to be accounted for. Being able to measure it directly would therefore be ideal to correct for this type of distortions. Such an approach was first introduced in 2003 [33] and resulted in a series of multiphoton intrapulse interference phase scan (MIIPS) methods [34-36], which can be described also as reference-based pulse characterization and compression.

The MIIPS technology is a single-beam approach that incorporates the diagnostics, pulse compression, and shaping functionalities into a single modular device. It takes advantage of a calibrated pulse shaper to measure the unknown spectral phase. The principle is to introduce a known reference phase and observe the interference that such a phase causes for some nonlinear optical process. For example, the presence of a phase with a cubic dependence on frequency leads to narrowing of the SHG spectrum around a local maximum at $2\omega_0$, where ω_0 is the frequency at which the second derivative of the phase crosses zero. The addition of a quadratic phase causes the spectral maximum of the SHG intensity to shift along with ω_0 . In fact, by scanning the SOD and collecting the SHG spectrum, one is able to obtain directly the second derivative of the phase accumulated by the pulse.

The accuracy that MIIPS methods are able to

achieve was not fully appreciated until 2007, when the dispersion of water was measured with accuracy and precision better than 0.5 fs^2 [37]. Those measurements were carried out by compensating the dispersion introduced by different path lengths of water, and the results proved to be more accurate than those obtained by white light interferometry. Since then, the dispersion of atmospheric gases and that of common solvents has also been measured [38, 39].

Commercially available products

Biophotonic Solutions Inc. (BSI) offers a wide range of customizable systems based on the 4f shaper design and MIIPS technology.

In close collaboration with the Dantus group at Michigan State University, BSI has demonstrated the delivery of $<8\text{fs}$ pulses at the microscope objective focus (see Fig. 4 and ref. [40]), the effect of high-order dispersion compensation on the efficiency of SHG and TPEF [41], as shown in Fig. 5, and the efficacy of using low-energy ultrashort pulses for nonlinear microscopic imaging of absorbing media [42].

To assist the growing number of MIIPS users in the nonlinear microscopy field, BSI introduced a microscope detection unit (MDU), which integrates the harmonic generation, filtering,

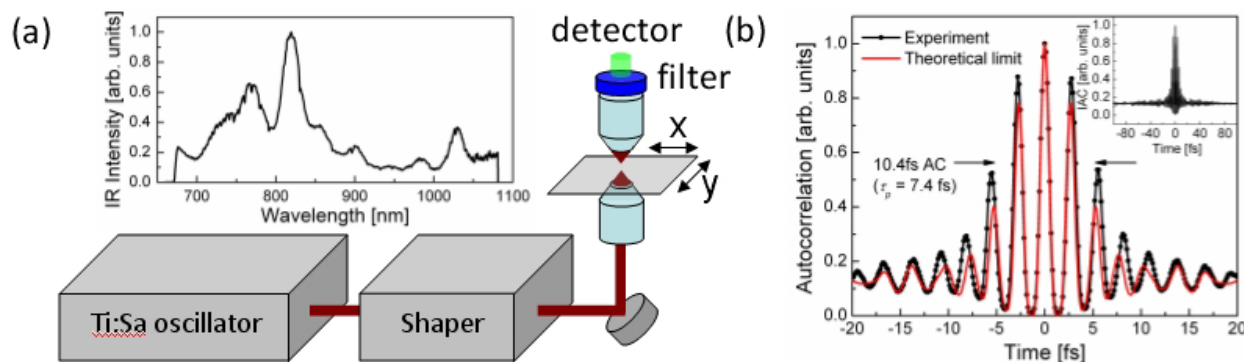


Figure 4. (a) Experimental setup layout based on a VENTEON oscillator and MIIPSBox640 shaper. Ocean Optics QE65000 spectrometer is used as a detector. The sample position is scanned by a XY piezo driver (PI Instruments). Inset: laser spectrum after the shaper; (b) Shaper-assisted interferometric autocorrelation trace obtained *in situ* at the focal plane of Nikon Plan Fluor ELWD 40x/0.60 objective. Inset: same IAC trace but over $\pm 100\text{fs}$ time span.

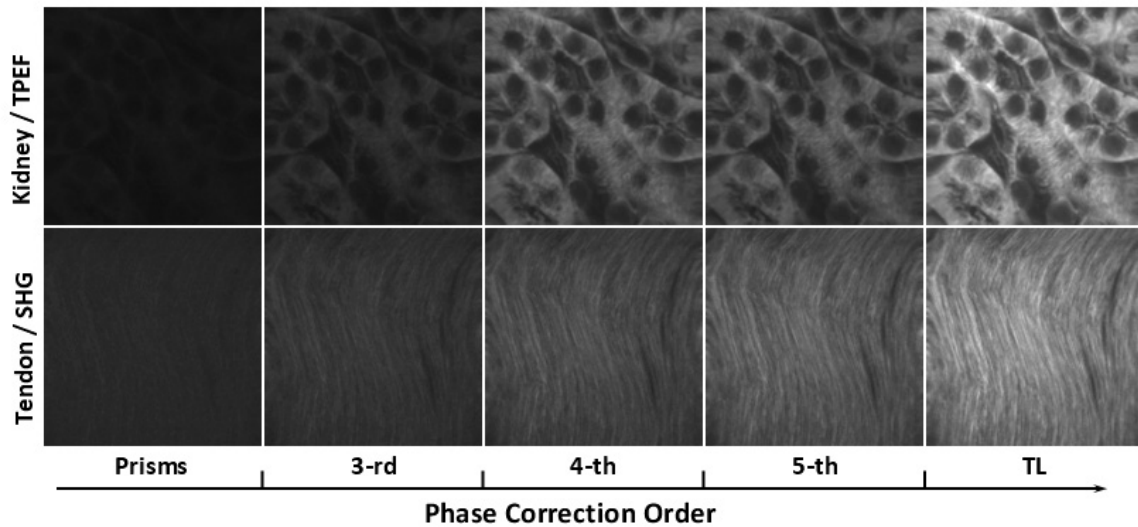


Figure 5. Effect of high-order phase distortions on signal intensity in 2PE fluorescence and SHG imaging. The SOD of the optical setup is compensated via a prism-pair compressor. Higher-order dispersion is accounted for by a 4f pulse shaper with a SLM in its Fourier plane. The residual spectral phase distortion, determined from a MIIPS scan, is fitted with a third, fourth, and fifth-order polynomials. The found phase functions are then programmed onto the SLM. TL pulses are obtained by full phase correction using MIIPS compensation mask. First row: 2PEF images of a fluorescently stained mouse kidney slide (Molecular Probes). Second row: SHG images of rat tendon, obtained for corresponding phase correction functions. All 512×512-pixel images are acquired for the same laser power of ~1 mW at the sample and averaged over 20 scans. The image size is 150μm×150μm. The objective used is water-immersion Zeiss LD C-APOCHROMAT 40x/1.1.

and fiber-coupled detection of the SHG signal in a small foot-print device that can be placed on the microscope sample holder; see Fig. 6.

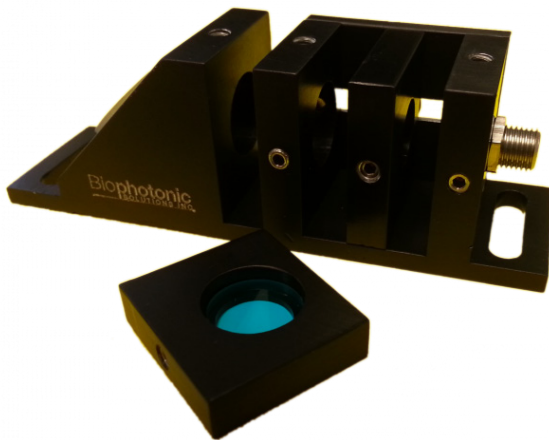


Figure 6. Microscope detection units, offered by BSI. A color filter is inserted to separate SHG from the fundamental laser beam. The filtered light is fiber-coupled into a spectrometer (not shown).

References

1. K. König, *Journal of Microscopy-Oxford* **200**, 83 (2000).
2. W. R. Zipfel, et al., *Nature Biotechnology* **21**, 1368 (2003).
3. F. Helmchen and W. Denk, *Nature Methods* **2**, 932 (2005).
4. J. N. D. Kerr and W. Denk, *Nature Reviews Neuroscience* **9**, 195 (2008).
5. E. Beaurepaire, et al., *Optics Communications* **188**, 25 (2001).
6. P. Theer, et al., *Opt. Lett.* **28**, 1022 (2003).
7. P. Theer and W. Denk, *JOSA A* **23**, 3139 (2006).
8. I. Pastirk, et al., *Opt. Express* **11**, 1695 (2003).
9. J. P. Ogilvie, et al., *Opt. Express* **14**, 759 (2006).
10. K. Isobe, et al., *Opt. Express* **17**, 13737 (2009).
11. P. Xi, et al., *J. Biomed. Opt.* **14**, 014002 (2009).
12. C. Soeller and M. B. Cannell, *Pflugers Archiv-European Journal of Physiology* **432**, 555 (1996).
13. S. Tang, et al., *J. Biomed. Opt.* **11**, 020501 (2006).
14. P. Xi, et al., *Optics Communications* **281**, 1841 (2008).
15. M. Müller, et al., *J Microsc* **191**, 141 (1998).

16. M. Muller, et al., *J Microsc* **191**, 141-150 (1998).
17. R. L. Fork, et al., *Opt. Lett.* **12**, 483 (1987).
18. A. M. Larson and A. T. Yeh, *Opt Lett* **31**, 1681 (2006).
19. E. A. Gibson, et al., *Opt. Lett.* **31**, 3363 (2006).
20. J. B. Guild, et al., *Applied Optics* **36**, 397 (1997).
21. R. Wolleschensky, et al., *Applied Physics B-Lasers and Optics* **67**, 87 (1998).
22. C. Froehly, et al., *Prog in Optics* **20**, 65 (1983).
23. A. M. Weiner, et al., *JOSA B* **5**, 1563 (1988).
24. M. Haner and W. S. Warren, *Appl Phys Lett* **52**, 1458 (1988).
25. M. E. Fermann, et al., *Opt. Lett.* **18**, 1505 (1993).
26. F. Verluise, et al., *Opt. Lett.* **25**, 575 (2000).
27. T. Baumert, et al., *Appl Phys B* **65**, 779 (1997).
28. D. Meshulach, et al., *Optics Communications* **138**, 345 (1997).
29. A. Galler and T. Feurer, *Appl Phys B* **90**, 427 (2008).
30. N. Forget, et al., *JOSA B* **27**, 742 (2010).
31. B. von Vacano, et al., *JOSA B* **24**, 1091 (2007).
32. D. Pestov, et al., *Opt. Lett.* **35**, 1422 (2010).
33. M. Dantus, et al., *OE Magazine* **9**, 15 (2003).
34. V. V. Lozovoy, et al., *Opt. Lett.* **29**, 775 (2004).
35. B. W. Xu, et al., *JOSA B* **23**, 750 (2006).
36. V. V. Lozovoy, et al., *Opt. Express* **16**, 592 (2008).
37. Y. Coello, et al., *Applied Optics* **46**, 8394 (2007).
38. P. J. Wrzesinski, et al., *Opt. Express* **19**, 5163 (2011).
39. P. Devi, *AIP Advances* **1**, 032166 (2011).
40. D. Pestov, et al., "Two-Photon Microscopy with Sub-8fs Laser Pulses," in *Frontiers in Optics*, OSA Technical Digest (CD) (Optical Society of America, 2010), PDPA4.
41. Y. Andegeko, et al., *Ultrafast multiphoton microscopy with high-order spectral phase distortion compensation* (SPIE, 2009), Vol. 7183, p. 71830W.
42. D. Pestov, et al., *J. Opt.* **12**, 084006 (2010).

For further information about BSI products, please contact us:

Biophotonic Solutions Inc.
1401 East Lansing Drive, Suite 112
East Lansing, MI 48823, USA

Phone: +517-580-4075
Fax: +517-579-8571
E-mail: info@bsifemto.com

www.biophotonicsolutions.com

This White Paper has been prepared based on research and development activities at Biophotonic Solutions Inc. Actual results may vary based on laboratory environment and setup conditions, the type and condition of actual components and instruments used and user skills.

Nothing contained in this White Paper shall constitute any representation or warranty by Biophotonic Solutions Inc., expressed or implied, regarding the information contained herein or the products or software described herein. Any and all representations, warranties and obligations of Biophotonic Solutions Inc. with respect to its products and software shall be as set forth in Biophotonic Solutions Inc. terms and conditions of sale in effect at the time of sale or license of such products or software. Biophotonic Solutions Inc. shall not be liable for any costs, damages and expenses whatsoever (including, without limitation, incidental, special and consequential damages) resulting from any use of or reliance on the information contained herein, whether based on warranty, contract, tort or any other legal theory, and whether or not Biophotonic Solutions Inc. has been advised of the possibility of such damages.

Users of the products or software described herein should refer to the User's Manual and other documentation accompanying such products or software at the time of sale or license for more detailed information regarding the handling, operation and use of such products or software, including but not limited to important safety precautions.

This White Paper shall not be copied, reproduced, distributed, transmitted, displayed, or published, in whole or in part, without the prior written permission from Biophotonic Solutions Inc.

Copyright ©2011-2015 Biophotonic Solutions Inc. All Rights Reserved. Our products, the MIIPS® technology and its use may be covered by one or more of the following US patents: 7,105,811; 7,439,497; 7,450,618; 7,567,596; 7,583,710; 7,609,731; 7,973,936; European patents: EP 1,723,704 as well as other US or international patents pending.